UPPSALA
UNIVERSITET

Dosimetry Studies of Different Radiotherapy Applications using Monte Carlo Radiation Transport Calculations

SHIRIN ABBASINEJAD ENGER

ACTA
UNIVERSITATIS
UPSALIENSIS
UPPSALA
2008

Dissertation presented at Uppsala University to be publicly examined in Fåhreussalen, C5, Rudbecklaboratoriet, Dag Hammarskjölds väg 20, Uppsala, Saturday, October 11, 2008 at 09:15 for the degree of Doctor of Philosophy (Faculty of Medicine). The examination will be conducted in English.

Abstract
Abbasinejad Enger, S. 2008. Dosimetry Studies of Different Radiotherapy Applications using Monte Carlo Radiation Transport Calculations. Acta Universitatis Upsaliensis. *Digital Comprehensive Summaries of Uppsala Dissertations from the Faculty of Medicine* 375. 49 pp. Uppsala. ISBN 978-91-554-7279-5.

Developing radiation delivery systems for optimisation of absorbed dose to the target without normal tissue toxicity requires advanced calculations for transport of radiation. In this thesis absorbed dose and fluence in different radiotherapy applications were calculated by using Monte Carlo (MC) simulations.

In paper I-III external neutron activation of gadolinium (Gd) for intravascular brachytherapy (GdNCB) and tumour therapy (GdNCT) was investigated. MC codes MCNP and GEANT4 were compared. MCNP was chosen for neutron capture reaction calculations. Gd neutron capture reaction includes both very short range (Auger electrons) and long range (IC electrons and gamma) products. In GdNCB the high-energetic gamma gives an almost flat absorbed dose delivery pattern, up to 4 mm around the stent. Dose distribution at the edges and inside the stent may prevent stent edge and in-stent restenosis. For GdNCT the absorbed dose from prompt gamma will dominate over the dose from IC and Auger electrons in an in vivo situation. The absorbed dose from IC electrons will enhance the total absorbed dose in the tumours and contribute to the cell killing.

In paper IV a model for calculation of inter-cluster cross-fire radiation dose from β-emitting radionuclides in a breast cancer model was developed. GEANT4 was used for obtaining absorbed dose. The dose internally in cells binding the isotope (self-dose) increased with decreasing β-energy except for the radionuclides with substantial amounts of conversion electrons and Auger electrons. An effective therapy approach may be a combination of radionuclides where the high self-dose from nuclides with low β-energy should be combined with the inter-cell cluster cross-fire dose from high energy β-particles.

In paper V MC simulations using correlated sampling together with importance sampling were used to calculate spectra perturbations in detector volumes caused by the detector silicon chip and its encapsulation. Penelope and EGSnrc were used and yielded similar results. The low energy part of the electron spectrum increased but to a less extent if the silicon detector was encapsulated in low z-materials.

Keywords: External Beam Radiotherapy, Gadolinium Neutron Capture Therapy, Gadolinium Neutron Capture Brachytherapy, Targeted Radionuclide therapy, Detector Response Modelling, Monte Carlo Simulation.

Shirin Abbasinejad Enger, Department of Oncology, Radiology and Clinical Immunology, Biomedical Radiation Sciences, Rudbecklaboratoriet, Uppsala University, SE-75185 Uppsala, Sweden

List of papers

This thesis is based on the following papers, which will be denoted by their roman numerals when referred to in the text.

I   Enger SA, Munck af Rosenschöld P, Rezaei A, Lundqvist H. Monte Carlo calculations of thermal neutron capture in gadolinium: a comparison of GEANT4 and MCNP with measurements. Med Phys. 2006 Feb;33(2):337-41.

II   Enger SA, Rezaei A, af Rosenschöld PM, Lundqvist H. Gadolinium neutron capture brachytherapy (GdNCB), a new treatment method for intravascular brachytherapy. Med Phys. 2006 Jan;33(1):46- 51.

III   Enger SA, Fortin MA, Lundqvist H, Munck af Rosenschöld P. Dosimetry for Gadolinium Neutron Capture Therapy (GdNCT). Submitted.

IV   Enger SA, Hartman T, Carlsson J, Lundqvist H. Cross-fire doses from ß-emitting radionuclides in targeted radiotherapy. A theoretical study based on experimentally measured tumor characteristics. Phys. Med. Biol. 2008 April; 53:1909-1920.

V   Eklund K, Enger SA, Ahnesjö A. Determination of self perturbations of spectra in detectors in photon fields. Manuscript.

Contents

Abbreviations

Intravascular Brachytherapy	IVBT
Monte Carlo	MC
Electron Gamma Shower	EGS
PENetration and Energy LOss of Positrons and Electrons	Penelope
Monte Carlo N-Particle Transport Code System	MCNP
GEometry ANd Tracking Version 4	GEANT4
Percutaneous Transluminal Angioplasty	PTA
Percutaneous Transluminal Coronary Angioplasty	PTCA
In Stent Restenosis	ISR
Gadolinium	Gd
Gadolinium Neutron Capture Brachytherapy	GdNCB
Linear Energy Transfer	LET
Electron Capture	EC
Internal Conversion	IC
Gadolinium Neutron Capture Therapy	GdNCT
Quality Assurance	QA
Variance Reduction Techniques	VRT
Neutron Capture therapy	NCT
Condensed History Technique	CHT
Evaluated Nuclear Data Files	ENDF
Magnetic Resonance Imaging	MRI
Boron Neutron Capture Therapy	BNCT
Polymethylmethacrylate	PMMA
Neutron Capture Reactions	NCR
Gd Neutron Capture Reactions	GdNCR

Introduction

Cancer and cardiac diseases are the main causes of death in the developed countries. For cancer, radiation therapy alone or combined with chemotherapy and surgery, is used to treat patients with curative intent, and has also an important role for palliation of symptoms from cancer. Independent of the application area, the aim of radiation therapy is to give an adequate radiation absorbed dose to the volumes containing malignant cells (the target) while minimising the dose to healthy tissue. Due to scientific and technological advances in the last decades, important steps in providing tools for effective and successful cancer treatment have been made. Development of imaging modalities has made it possible to detect cancer early, accurately diagnose it and improve the definition of target volumes or healthy tissue at risk. The growth in computer processing power and technology has enabled development of sophisticated three-dimensional treatment planning systems. Many strategies have been developed for delivering beams used in external radiotherapy. Beside the commonly used linear accelerators delivering high-energy photon and electron beams, proton beams are becoming more available and light ions are under development in several research centres.

The use of external radiation therapy may be limited in cases where the proximity of the target volumes to radiosensitive normal tissues makes it difficult to obtain an optimal absorbed dose distribution in the target. Approaches such as brachytherapy and targeted radionuclide therapy where the radiation sources are concentrated in the target volume are therefore also of interest.

Since radiation induce cell killing and prevents tissue growth, it can also be used in cardiology to treat restenosis in blood vessels after balloon angioplasty and stenting. In intravascular brachytherapy (IVBT), radiation sources are applied directly to the site of narrowed vessels and arteries to kill the cells that have re-closed the stent and to prevent further restenosis by inhibiting tissue growth [1-5].

In targeted radionuclide therapy one uses radiolabeled tumour-targeting molecules to selectively deliver therapeutic doses. This technique is of particular interest for primary tumour and disseminated tumour cells and metastases that are too small for surgery or external radiotherapy [6-9].

The development of new radiation therapy systems requires advanced calculations for analysing the transport of radiation through the body and components of the treatment devices themselves. The Monte Carlo (MC)

method is a detailed and accurate method for calculation of fluence and absorbed dose distributions. Implementing the MC method for simulation of radiation transport in matter has lead to the development of several general purpose codes such as EGSnrc (Electron Gamma Shower) [10], Penelope (PENetration and Energy LOss of Positrons and Electrons) [11], MCNP (Monte Carlo N-Particle Transport Code System) [12] and GEANT4 (GEometry ANd Tracking version 4) [13]. It is important to compare different MC codes against experiments to evaluate the relevance and accuracy of the calculated results.

In this work, absorbed dose and particle fluence for selected problems in external beam radiotherapy, IVBT, targeted radionuclide therapy and detector response modelling have been calculated by MC simulations. To validate the results a number of MC codes were compared, and for some cases the calculated results were compared to benchmark experiments. A more detailed description of the studied applications will be discussed in the next section.

Specific applications studied

In this thesis new techniques for delivering absorbed dose ranging from external beam radiotherapy, IVBT, targeted radionuclide therapy, and detector response modelling are investigated by use of the MC method.

Intravascular Brachytherapy

A common cardiac vascular disease is narrowed or blocked vessels (stenosis). Percutaneous transluminal angioplasty (PTA) and percutaneous transluminal coronary angioplasty (PTCA) refers to techniques of dilating (opening) blocked vessels from inside. In balloon angioplasty a deflated balloon catheter is placed inside the narrowed segment of the vessel. The vessel is stretched open by inflating the balloon and thereby pressing the plaque against the vessel wall. [14] During balloon angioplasty a metal mesh tube (stent) can be placed inside the vessel to keep it open and to prevent future blockage. [15]

The tissue stress created by the stenting procedure may start a cell proliferation called intimal hyperplasia, which in a substantial fraction of patients may lead to a so-called in stent restenosis (ISR). This is the major side effect of balloon and/or stent angioplasty. Ionising radiation can be used to decrease the cell proliferation leading to restenosis. IVBT is a technique where the radiation dose is applied locally by several ways, like placing balloons with radioactive solutions inside the stent area as well as radioactive wires, radioactive seeds and radioactive stents. [1-5]

However, IVBT has some specific problems. One is that the radiation source has to be applied in the same session as the PTC/PTCA using the same catheter system. Thus, the radiation source (stent, wire etc) has to be correctly positioned under stress in order to get the wanted dose distribution. The number of involved specialists, the time factor, and the radiation risk to the personnel complicates the procedure and increases the risk of failures. Furthermore, with the current techniques the radiation dose can be delivered only once and during the catheterisation procedure, but radiation will have a better effect a couple of days after the invention when the cells starts to proliferate. Due to the complexity of performing IVBT, the use of this application has been decreased during the last years in benefit for drug eluting stents with a much simpler placement and good results in decreasing ISR [16].

In this work external activation of gadolinium (Gd) by thermal neutrons has been investigated as an alternative treatment method for IVBT. The method is called Gd neutron capture brachytherapy (GdNCB) and offers several advantages compared to the previous radiation techniques. By inserting non-radioactive Gd stent radiation hazards to personnel can be avoided. Activation of the stent by an external neutron field can be performed days after catheterisation when the target cells start to proliferate and can be expected to be more radiation sensitive. The position of the stent can be verified and corrected by the treatment plan prior to activation. Fractionation of the absorbed dose is possible through multiple activations and will spare normal tissue. For activation of Gd by thermal neutrons and absorbed dose calculations two different MC codes, MCNP and GEANT4 were compared.

Targeted radionuclide therapy

Targeted radionuclide therapy is a form of radiotherapy using radio-labeled tumour-targeting molecules to selectively deliver therapeutic doses of ionising radiation to both a primary tumour and disseminated tumour cells and metastases. This is of particular interest when the tumours are too small to be identified as candidates for surgery or external radiotherapy [6-9].

An important factor in targeted radiotherapy is the selection of the radionuclide. Depending on the size of the targeting molecule the time to reach the maximal uptake can vary considerably. For a successful therapy the tumour must have a higher uptake and/or longer retention time of the radionuclide than normal tissue, which means that the physical half-life has to be in the same order as the typical biological distribution times. But also other physical properties of the radionuclide are important. A high fraction of the radiation energy emitted should be absorbed in the tumour tissue, which means that the radionuclide of choice should have an appropriate energy deposition profile to irradiate large tumours as well as micro-metastases and single cancer cells. To compensate for the heterogeneous radionuclide distribution, the irradiating particle should have long enough range. Due to such demands several types of radionuclides with different linear energy transfer (LET) have been suggested for use in targeted radionuclide therapy i.e. α-emitting radionuclides, β-emitting radionuclides, conversion and Auger electron emitting radionuclides.

α-emitting radionuclides

Radionuclide emitted α-particles are high-LET particles with energies in the range of 5 to 9 MeV, which corresponds to particle ranges in the order of several cell diameters. Hence, use of α-particle nuclides do not necessarily require internalisation into all target cells since irradiation of untargeted cells

by radionuclide bound to adjacent targeted cell may kill neighbouring tumour cells with no radionuclide uptake (cross-fire effect).

β-emitting radionuclides

Radionuclide emitted β-particles are low-LET particles with a continuous spectrum of energies ranging from zero up to a maximum energy. The path length varies from several tens to hundreds of cell diameters. The long path length of β-particles is an advantage when targeting large tumours with sizes well above the range of the β-particles since not all cells need to be targeted.

Auger electrons

For radionuclides that decay by electron capture (EC) and internal conversion (IC) processes, inner shell electron vacancies are created which are filled by electronic transitions from shells of higher energy. Due to differences in electron energy each inner-shell electron transition results in the emission of a characteristic X-ray photon or Auger electrons. Individual Auger electrons are low-LET radiation but the simultaneous emission of several Auger electrons with nanometre range can causes biological damage similar to that of high-LET radiation. Due to the short range of such particles the radioactive decay has to be close to, or preferable from an atom incorporated into the DNA molecule.

Conversion electrons

After a radioactive decay the daughter nuclide might end up in an excited state. In the de-excitation process either gamma photons or conversion electrons are emitted. Depending on the energy of the excited state the energy of the conversion electrons may vary from tens of keV to MeV.

In this work targeted radionuclide therapy was investigated in two studies. In Gd neutron capture therapy (GdNCT), a selective therapeutic effect can be achieved by targeting sufficient amounts of ^{157}Gd nuclide to the target tumour cells. The capture of neutrons by ^{157}Gd provokes a succession of complex decay transitions that generate a low-LET prompt gamma spectra ranging from 0.08 MeV to 7.8 MeV. This is accompanied by the emission of internal conversion electrons ranging in energy from 79 keV to 6.9 MeV. These electrons leave orbital electron vacancies that de-excite by emitting X-rays or low-energy Auger electrons. The therapeutic dose delivered microscopically (to nearby cells) by short-range low-energy electrons and macroscopically, by long-range gamma rays, at given distances from the radiation emission site has been investigated. Transport calculations of the activating

neutron beam were performed by the MC code MCNP. GEANT4 was used for the induced electron/gamma transport cascade following the activated nuclide decay.

In the second study estimation of inter-cluster cross-fire radiation dose from different β-emitting radionuclides in a breast cancer model was presented in a model designed on the basis of histological findings. All the calculations in that study were performed by means of the GEANT4 MC code.

Detector response modelling

The delivery of absorbed dose in radiotherapy requires efficient tools and methods for dosimetry and quality assurance (QA) to verify that the delivered dose is the same as the dose calculated by treatment planning system. Diode detectors are used in both *in vitro* and *in vivo* dosimetry. Silicon diodes used for dosimetry in QA are provided with encapsulation that must be appropriately chosen depending on the type and quality of the clinical beams. Until now, the designs of diode-encapsulations are the result of empirical investigations of detector properties, and no thorough calculations have been done to analyse its influence on the particle spectrum inside the active volume and optimise the designs.

In this thesis the spectra perturbations inside a silicon diode detector caused by the silicon chip and its encapsulation was investigated using Monte Carlo simulation packages Penelope and EGSnrc.

Monte Carlo Method for radiation transport

In many areas dealing with ionising radiation, it is important to calculate three dimensional radiation transport through matter. In principle the Boltzmann equation gives a differential equation description of the transport of radiation particles. However, there is no general analytical solution to the Boltzmann transport equation but numerical solution methods exist, often involving approximate methods that are compromises between physical accuracy and feasibility. Two distinct approaches have been developed: deterministic methods [17, 18] and stochastic methods i.e. MC methods [19-24].

MC methods are numerical methods based on random sampling. General principles of the MC method are described in detail in a number of publications and will not be discussed in detail here. [19, 20] The key to MC methods is to relate computer generated random numbers to physical events through the probability density functions of the possible interactions, i.e. the cross section values. Hence, MC codes must include cross section libraries for calculating the probability of a particle interacting with the medium through which it is transported. The cross section for each interaction is dependent on the incident particle, its energy, and the material it travels through.

Simulated particles are followed as they lose energy, generate other particles, and ultimately 'killed' as they either escapes from the geometry of interest or their energy falls below a given threshold. During this process, quantities such as fluence or absorbed dose can be scored. The scored quantities are estimates, which lie within confidence intervals corresponding to certain probabilities. The uncertainty associated with the result is a function of the number of particle histories simulated. By running more histories, the uncertainty gets smaller, usually following a $1/N^{1/2}$ relation.

Since simulating more histories in MC calculations are time consuming, different techniques called variance reduction techniques (VRT) are often used to improve the calculation efficiency. The efficiency, ε, of a MC calculation has been defined as: $\varepsilon=1/(\sigma^2 t)$, where t is the CPU time required to obtain the variance σ^2 of the quantity of interest [25]. The efficiency of MC simulations can be increased by either reducing the resulting variance, or by decreasing the CPU time per particle simulated.[25-28] MC codes usually include specific VRT for each particle type but some general methods are also available. Correlated sampling is a VRT technique that can be used in the transport of both photons and electrons. When differences between simu-

lated geometries or media is small, and the ratio of, or difference between, certain quantities due to the differences in the simulation geometries, is of interest, correlated sampling is very useful. The uncertainties in the ratios of the calculated results and the differences obtained with correlated sampling are, in general, smaller than those obtained from uncorrelated simulations [29-32].

All of the general purpose MC codes used in this study simulate photon and electron transport. The main difference between the codes depends on the use of different cross section libraries and physical interaction models [33-38]. In some areas in radiotherapy such as neutron capture therapy (NCT) it is necessary to simulate also neutron transport. MCNP and GE-ANT4 are two MC codes that are appropriate for neutron transport simulations.

Photon transport

In photon transport the distance s (step length) to the next interaction in a medium is calculated by:

$$s = \lambda \ln(1-\xi)$$

where $\lambda = (1/\mu)$ is the mean free path for the photon energy at the beginning of the step, μ (cm^{-1}) is the linear attenuation coefficient and ξ is a random number. The type of interaction occurring after the step s is dependent on the photon energy and is sampled from the probabilities for interaction. Having done this, the surviving particles have their energies, directions and other characteristics chosen from the appropriate distributions.

The interaction processes important for radiotherapy applications are incoherent (Compton) scattering, coherent (Rayleigh) scattering, photoelectric effect and pair production. The photonuclear interactions occur only for photon energies above a few MeV and are of less importance in most applications. [39]

Electron transport

Electrons and positrons interact with surrounding media via elastic scattering, inelastic collisions and bremsstrahlung emission. Positrons can also undergo annihilation either in flight or at rest. [39]

Direct simulation of electron transport is demanding due to the large number of interactions (10^5-10^6 collisions per particle) in the slowing down process. Berger [40] developed a condensed history technique (CHT) to avoid the simulation of all the physical interactions. Multiple scattering theories used in CHT utilise that most electron interactions result in extremely

small changes in energy and/or direction and that the macroscopic effect of a large number of electron interactions can be condensed into a single step of a certain "step-size", expressed either as the distance travelled, or energy lost during a CHT transport step.

CHT is classified in two procedures: Class I and Class II. Class I algorithms groups all the interactions, and transport electrons along a predetermined pathlength. Random sampling of the interactions is performed at the end of the step. Class II algorithms use a mixed procedure, where interactions with small energy losses or deflections are grouped together while interactions causing large energy loss or deviations are sampled individually and angular deviations are treated more accurately in this way. The correlation between energy loss and angular deflection can be conserved with the random hinge method [41].

Differences between the physical interaction models and cross sections for electron and photon transport adopted in general purpose MC codes used in this thesis are given in a review by Frank Verhaegen and Jan Seuntjens. [42]

Differences in neutron cross section in MCNP and GEANT4

MCNP is a general purpose code that can be used for neutron, photon, electron, or coupled neutron/photon/electron transport. GEANT4 was originally implemented for high-energy physics applications and is known to handle particle transport at high energies well but its capacity to simulate low-energy neutron transport is not equally well tested. In MCNP thermal neutrons are described both by the thermal neutron scattering from chemically bound atoms $S(\alpha,\beta)$ and free atom models, while in GEANT4 only the free atom model is used. The main difference between the bound and free models is the distribution of secondary neutrons in direction and energy, since thermal motion changes the direction and speed of scattered neutrons. At thermal neutron energies, the chemical binding of the scattering nucleus in a solid, liquid, or gas target material affects the neutron cross section and the energy and angular distribution of secondary neutrons, as the incident neutrons can lose or gain energy differently in interactions with the target molecules. In the evaluated nuclear data files (ENDF) used by MCNP these effects are described in the thermal sub library where $S(\alpha,\beta)$ is parameterised in terms of momentum transfer parameter α and energy transfer parameter β. With this model thermal scattering can include atomic translational motion as well as vibration and rotation. In the free atom model, thermal atomic motion is assumed to be Maxwellian. In both models the thermal motion changes the relative speed between target atoms and incident neutrons, which means that the reaction rate is changed [43].

Current study

The specific aims of this study were:

- to compare the commonly used code MCNP for neutron transport calculations with GEANT4, for NCT applications, paper I;
- calculating absorbed dose from gadolinium neutron capture reaction in brachytherapy, paper II;
- calculating absorbed dose from gadolinium neutron capture reaction for tumour therapy, paper III;
- calculating cross-fire doses from ß-emitting radionuclides in targeted radiotherapy, paper IV;
- calculation of spectra perturbations inside a silicon diode detector caused by the silicon chip and its encapsulation ,paper V;

Gadolinium capture therapy (Paper I, II and III)

Background

Neutron capture therapy (NCT)

In NCT a stable nuclide is introduced in the target volume either as a brachytherapy source or by local or systemic administration as in targeted radionuclide therapy. The nuclide is then activated by an external low-energy neutron source [44]. Several nuclides have properties that make them candidates for NCT. The nuclide of choice should concentrate in the target volume and have high absorption cross section of thermal neutrons causing prompt nuclear reactions. The quality of the radiation emitted should enable an efficient irradiation of the clinical target aimed for therapy. Example of such a nuclide is Gd, a paramagnetic metal with high thermal neutron capture cross section. Gd is already used clinically as contrast media for Magnetic Resonance Imaging (MRI).

NCT is simple in theory but in reality it demands a high technical quality of the involved components. The physical parameters involved are well known but interact in a rather complex way. One such factor is the production and delivery of the applied external neutron field. Thermal neutrons can not be used directly to irradiate deeply sited target volumes since they are strongly attenuated in the tissue. Therefore, due to their better penetration, epithermal neutrons have instead been employed. In the tissue they are slowed down by atomic collisions (primarily hydrogen) and a thermal neu-

tron fluence peak can be obtained at a greater depth. Thus, it is important that the beam delivery system produces sufficiently high amount of epithermal neutrons of right energy and with a low contamination of other radiation such as fast neutrons and gamma. Fast neutrons deliver absorbed dose by producing recoil protons when neutrons scatter in hydrogen. Thermal neutrons will cause nuclear reactions in normal tissue mainly through ^{14}N(n, p)^{14}C and ^{1}H(n,γ)^{2}H. The cross sections of these reactions are small compared to that of Gd, but the number of H and N atoms are considerably higher, and their contribution has to be considered in the evaluation.

Gadolinium

Natural Gd (seven stable isotopes) has a thermal neutron cross section of 49 000 barns. Gd neutron absorption reaction yields a wide spectrum of secondary radiation via low-energy conversion electrons, Auger electrons, X-rays, and high-energy gamma rays. While the Q values for these products range from 5.6 MeV to 8.6 MeV, depending on the Gd isotope, the majority of this energy is emitted as gamma rays, which have long mean free paths.

One of the isotopes, ^{157}Gd (15.7 % abundance), has the highest known thermal neutron cross section of any stable isotope (2.54×10^{5} barns). Thermal neutron capture in ^{157}Gd causes an exited state of ^{158}Gd which decays to the ground state through IC by emission of gamma rays. A few percent of the energy is converted to conversion electrons causing orbital electron vacancies that de-excite by emitting X-rays or Auger electrons. [45] The Auger electrons are highly ionising in the cellular or sub-cellular range. In order to induce double-strand breaks in the DNA the source must not just be placed in the cell nucleus but also attached to or placed within the DNA. Regardless of the fact that ^{157}Gd emits Auger electrons its qualities as a gamma emitter makes it interesting for brachytherapy.

The neutron beam

A model of the Studsvik boron neutron capture therapy (BNCT) facility was simulated by using MCNP and validated toward measurements at the exit of the filtering system. The reactor geometry is divided into three regions. The neutron spectra used as input data in the papers I-III is scored at the end of region II (figure 1), which means that our simulations include the last part of the beam line, i.e. a collimator delimiting a 14x10 cm^2 field and an eight mm thick ^{6}Li filter as it is illustrated in figure 1.
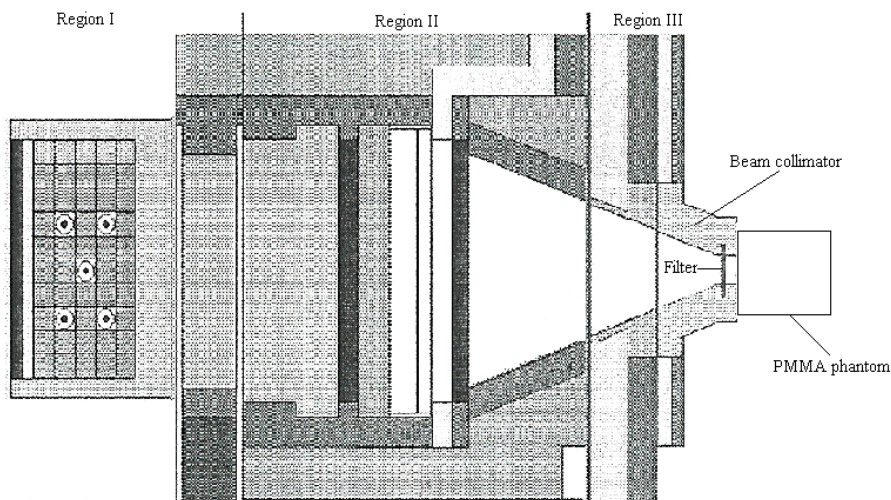
Figure 1. A schematic illustration of the beam filter and beam collimators at Studsvik viewed from above. Region I include the reactor core, a 20 cm thick Al layer and the Cd shield. Region II starts after the Cd shield and extends to the end of the first Pb collimator section. Our simulations start in region III, which includes the last part of the beam line, i.e. a collimator delimiting a 14x10 cm^2 field and 8 mm thick ^{6}Li filter. A 15x20x20 cm^3 PMMA phantom is placed in front of the beam port.

The phantom

A 15x20x20 cm^3 polymethylmethacrylate (PMMA) phantom was placed in front of the beam port. This phantom was used in all papers since it has been used previously for calculations and measurement of thermal neutron fluence of the Studsvik clinical beam. A point at 3 cm depth in the phantom on the beam centreline was chosen as reference point. According to the MCNP calculations, this point is close to the depth of thermal neutron fluence rate maximum in the phantom. The Gd tubes in paper I, II and the tumour model in paper III were placed at 3 cm depth because of the thermal neutron fluence peak at this point.

Film dosimetry

Dosimetric films from GafChromic™ dosimetry media were placed tangential to the Gd containing volumes along the beam direction in paper I and III. Ionising radiation causes a chemical cross linking in the film which results in a colour change proportional to the radiation dose. GafChromic™ dosimetry media is composed of materials with low atomic numbers and will not alter the radiation field. Calibrating the radiochromic film required two steps, first converting the pixel values into optical density, second converting optical density into dose. Translating the optical density into accurate dose values requires calibration specific to the film type and radiation type. The films are calibrated using a radiation source with known dose rate.

20

Paper I

Thermal neutrons are in MCNP described both by the thermal neutron scattering from chemically bound atoms (S(α,β)) and free atom models, while in GEANT4 only the free atom model is used. The aim of paper I was to investigate the effects of scattering on thermal neutron transport by calculating the fluence with MCNP and GEANT4 at different depths in the phantom. The fluence was calculated in small spheres with 5 mm diameters, placed in x, y, and z positions with 1 cm distance between them. The calculated fluence was compared with measurements. Data from the MCNP simulations agreed well with the experimental results when the scattering law (S(α,β)) was taken into account (figure 2) while the GEANT4 results were 25% lower.
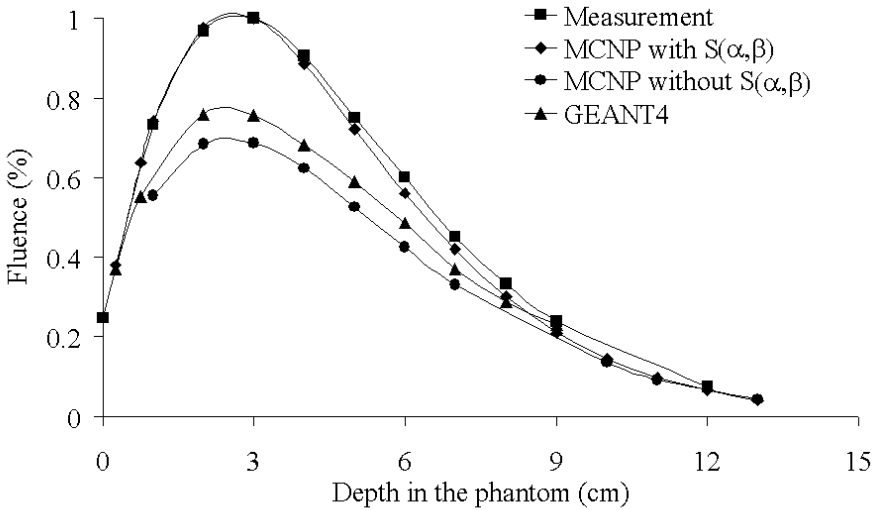
Figure 2. Relative thermal neutron fluence. The MCNP calculation with $S(\alpha,\beta)$ is normalised to the measurement on the beam centerline at the reference point of 3 cm. The MCNP and GEANT4 calculation without $S(\alpha,\beta)$ are also normalised at the reference point to the MCNP results that are normalised to the measurement. The statistical uncertainty is less than 1%. [46]

Sine thermal neutron fluence calculated with MCNP was in good agreement with measured fluence results, dosimetric film measurements and MCNP simulations were performed at the reference depth for a 25 µm thick natural Gd-foil shaped as a tube, 3 cm long and 5 mm in diameter. Relative dose distribution perpendicular to beam axis, tangential to the Gd tube is presented in figure 3. Each profile is individually normalised to the peak value.
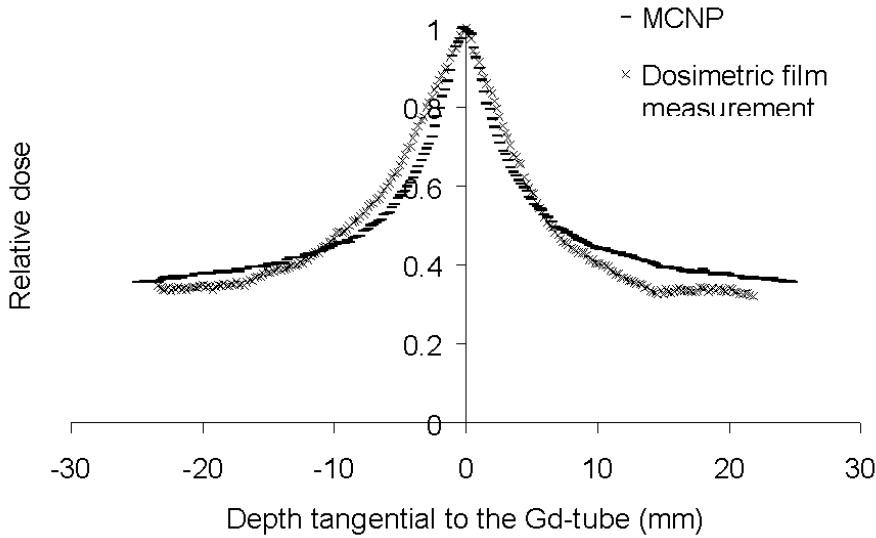
Figure 3. Relative dose distribution along the beam direction, tangential to the Gd tube. The tube is placed at the reference depth. Each profile is individually normalised to the peak value. The statistical uncertainty is 5%. [46]

Paper II

Paper II describes the possible use of Gd for GdNCB for treatment of restenosis. MCNP and GEANT4 MC codes were used to study capture rate, Kerma, absorbed dose and absorbed dose rate around Gd-containing stents activated with thermal neutrons. To study Gd containing stents, the simulated stents were located at 3 cm depth in a PMMA phantom with geometrical details as described in table 1, with epithermal neutron fluence as described above.

Table 1. Gd-tubes used in the calculations.

Length (cm)	Diameter (mm)	Thickness (μm)	Depth in the phantom (cm)
3	3	25	3
3	5	25	3
3	5	25	5
3	5	25	10

The Kerma from prompt gamma produced by the neutron capture reactions (NCR) in Gd was modelled. The absorbed dose from low-energy electrons were not considered in this study since the range of electrons with low-energy (<70 keV) is small and are not likely to leave the stent surface while

22

the abundance of conversion electrons of higher energies is only a few promille and will not significantly contribute to the absorbed dose. The relative number of thermal neutron captures for a cylindrical Gd-foil (diameter 5 mm, length 3 cm) as a function of thickness is presented in figure 4. The number of captures reached a plateau already after 10 μm and a foil of 5 μm thickness yields about 80% of the total number of captures. Although most of the calculations in this study were performed for a 25 μm thick Gd-foil, a thinner foil, between 5-10 μm thick would be ideal to use due to self shielding. The stent can be loaded with Gd in different ways, either incorporated as an alloy in the stent or as a thin, 5 μm foil between two stents.
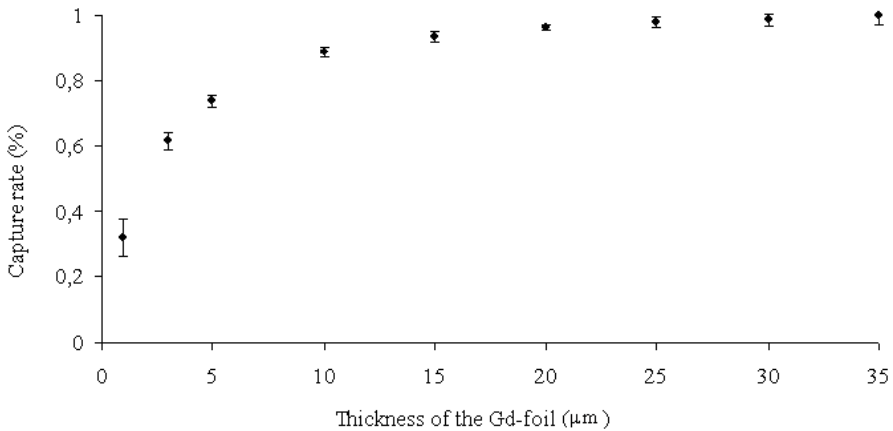
Figure 4. The relative number of neutron captures in a cylindrical natural Gd-foil (diameter 5 mm, length 30 mm) with varying thickness. The Gd-tube is placed in a phantom at 3 cm depth and irradiated with an epithermal field simulated with GEANT4. [47]

Three dimensional distribution of the neutron capture rate inside the wall of a 25 μm thick, 3 cm long Gd-tube with 5 mm diameter is given in figure 5. Normalisation was made to the highest capture value, which is at the outer surface of the Gd-tube. Thermal neutrons can reach and activate the inside of the stent edges. The higher capture rate at both ends leads to higher absorbed doses at the edges and inside the stent contributing to a non-uniform dose distribution and may counteract stent edge and ISR.
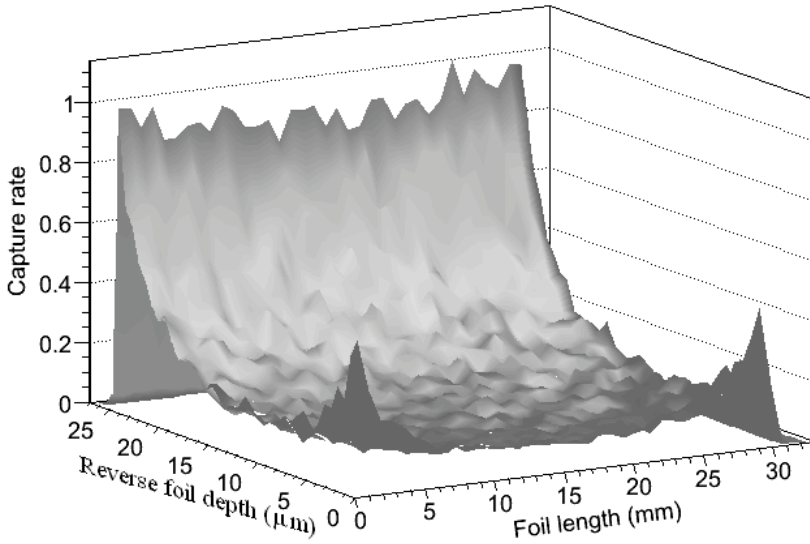
Figure 5. Relative capture rate in a 25 μm thick, 3 cm long Gd-foil with 5 mm diameter. The depth 25 μm is the outer surface of the Gd-foil while depth 0 is the inner surface of the foil i.e. the depth is reversed. The calculation is performed with GEANT4. [47]

To simulate Kerma from the Gd-tube as well as other radiation contributions, Gd-tubes with 3 and 5 mm diameters were placed inside the PMMA phantom at 3, 5 and 10 cm depths. The results are presented in figure 6a-6d. Photon dose from ^{1}H(n,γ)^{2}H and gamma contamination in the beam were the major contributors to the total dose the first centimetres of the phantom. The relation between maximum Kerma and the entrance Kerma increased from 0.47 at 3 cm depth to 0.56 at 5 cm depth to 0.85 at 10 cm depth. Since thermal neutron peak in tissue for the beam was at 3 cm depth, the Gd-tube placed at this position will yield higher amounts of Gd-associated gamma. At 5 and 10 cm depth the Gd associated gamma were fewer but also had a longer pathway to the surface and gave a relatively higher contribution to the entrance Kerma.
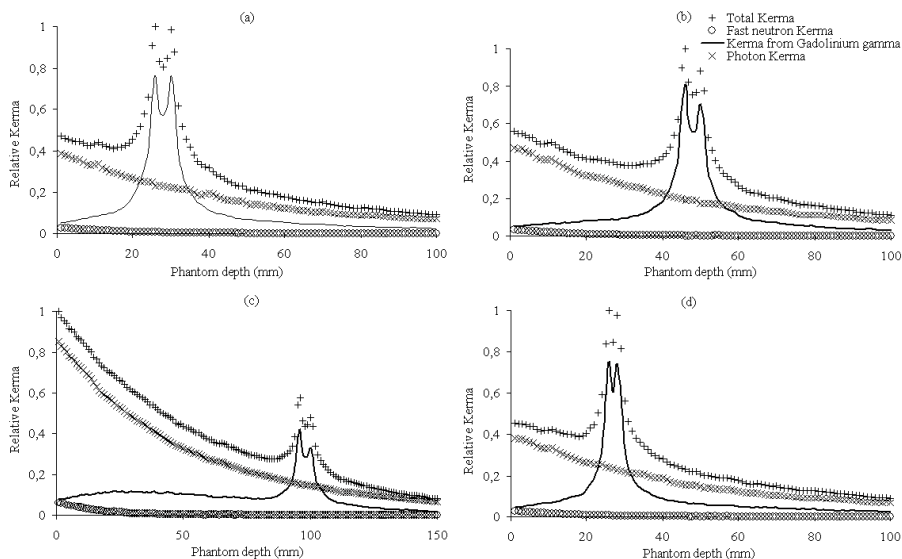
Figure 6. Relative Kerma distributions from different contributions for a (a) 3 cm long Gd-tube with 5 mm diameter placed at 3 cm depth in the phantom, (b) a 3 cm long Gd-tube with 5 mm diameter placed at 5 cm depth in the phantom, (c) a 3 cm long Gd-tube with 5 mm diameter placed at 10 cm depth and (d) a 3 cm long Gd-tube with 3 mm diameter placed at 3 cm depth in the phantom. All simulations are performed with MCNP. [47]

The dose distribution for the average gamma energy from Gd neutron absorption reaction was compared to dose distributions from two different mono-energetic (28 and 375 keV) gamma radiations to show the difference between low, intermediate, and high gamma energies. These energies were chosen to represent commonly used radio nuclides for IVBT (^{125}I and ^{192}Ir). The gamma radiations were sampled uniformly from the same geometry as the Gd-foil and presented in figure 7. Due to the build-up factor, high-energy photons gave a much better dose distribution around the vessel. The absorbed dose was almost flat the first 4 mm around the stent. In the application this means that the GdNCB-system can give an adequate dose to the target with a much less dose to the vessel wall. A slight drawback is that the integral dose due to the higher penetration of the high-energy gamma as well as to the neutron field will increase.
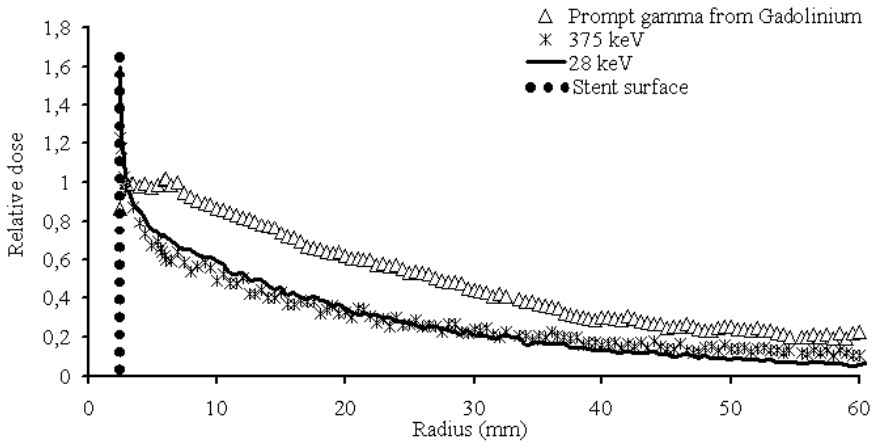
Figure 7. Relative radial dose distributions from high, intermediate and low gamma energy, normalised to 1 at 0.5 mm from the vessel wall simulated with GEANT4. [47]

Paper III

Paper III investigates the possibility to use Gd for tumour therapy. The background neutron dose as well as the prompt gamma dose from Gd neutron capture reaction (GdNCR) was calculated for Gd-containers with 1, 5, 15 and 30 mm diameter, 30 mm height and a concentration of 2000 ppm natural Gd, placed separately inside a PMMA phantom and exposed to epithermal neutron fluence described above. The uncertainties of the calculations were 1-3% (1SD). The absorbed dose was also measured for the largest container (30 mm in diameter). The MC calculations for obtaining the prompt gamma dose were performed with MCNP. The absorbed dose contribution from average energy of IC and Auger electrons from GdNCR were calculated with GEANT4 for a cell model.

The absorbed dose normalised to the maximum value and plotted as a function of depth in the phantom is presented in figure 8. The measured results agreed well with the calculated results for high doses but for low doses the measured results were higher than the calculated results. The difference between the prompt gamma dose and background dose decreased with the distance from the Gd-container. The background dose was induced by NCR in all elements except Gd. Thermal neutrons cause nuclear reactions in normal tissue mainly through $^{14}N(n, p)^{14}C$ and $^{1}H(n, \gamma)\,^{2}H$. The cross sections of these reactions are small compared to that of Gd, but the quantity of H and N atoms are considerably higher.
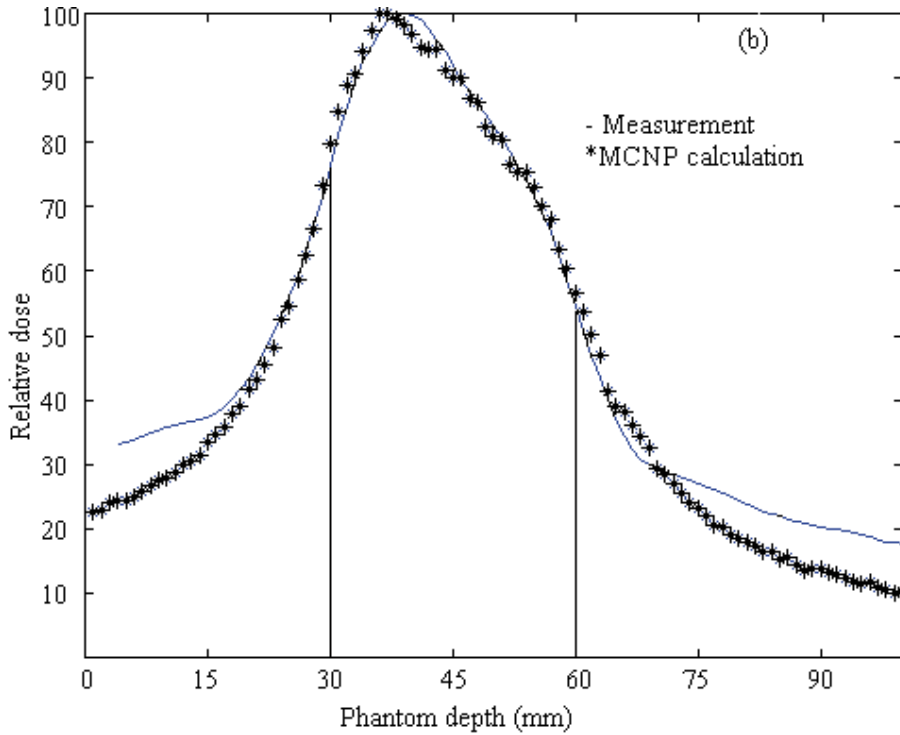
Figure 8. Absorbed dose measured for the largest container (30 mm in diameter) in percentage of maximum value plotted as function of position in phantom. Phantom was irradiated with Gd in the container (2000 ppm) by epithermal neutrons.

The calculated prompt gamma absorbed dose (Gy/h) with and without Gd in containers, with varying diameters as a function of phantom depth (cm) is shown in figure 9a. The Gd-containers had a concentration of 2000 ppm natural Gd and exposed to epithermal neutron beam. The prompt gamma absorbed dose was higher in large tumours than the absorbed dose in smaller tumours. The prompt gamma absorbed dose from GdNCR was at least 5 times higher than the background dose for the largest tumour (30 mm in diameter). The absorbed dose was high inside the tumour and decreased fast with the distance from the tumour due to the inverse square factor. The dose dropped twofold within 1 cm from the edge of the tumour and fell to the background level after 3 cm. The absorbed dose from the smallest Gd-container (1 mm in diameter, 3 cm length), which resembles a brachytherapy needle, was at the same level as the background dose. This was expected since the surface area of the container or needle affects delivery of the absorbed dose. Gd-containers with larger surface delivered higher dose.
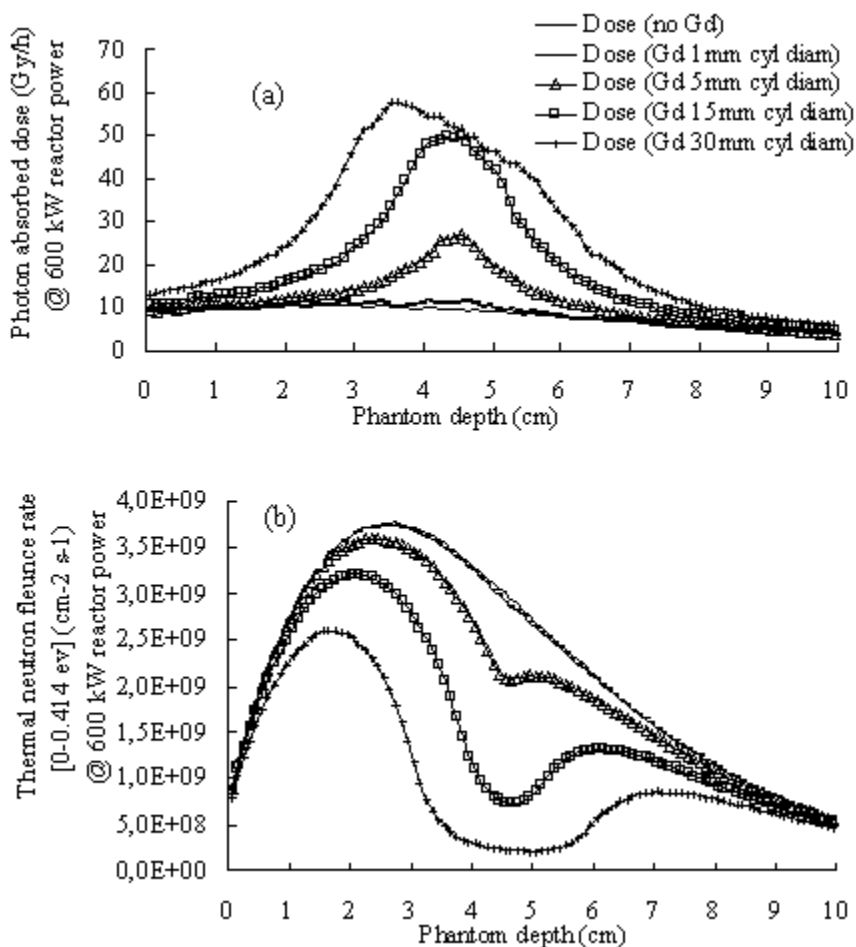
Figure 9.(a) MCNP calculated absorbed dose and photon kerma (Gy/hr) as a function of depth (cm). A PMMA phantom was irradiated with epithermal neutrons with and without a Gd-containing volumes (1, 5, 15 and 30 mm diameter, 30 mm height and a concentration of 2000 ppm natural Gd). (b) Thermal neutron fluence rate as a function of phantom depth with and without Gd-containing volumes.

Due to large Gd neutron absorption cross section there is a significant amount of thermal neutron fluence depression even at small amounts of Gd neutron capture compound present. Figure 9b illustrates thermal neutron fluence rate across the Gd-containers. As the volume of the container increased, the thermal neutron fluence rates across the volume decreased. The non-uniformity of the neutron fluence rate was significant for the largest tumour.

The absorbed dose contribution from average energy of IC-photon, IC-electron, fluorescence and Auger electrons was calculated for a cell model

28

with a radius of 6 μm and a nucleus with a radius of 1.5 μm, centred in the cell. Low-energy Auger electrons can increase the induction of complex double-strand breaks in the DNA if the source is attached to or placed within the DNA. Figure 10 illustrates the absorbed dose in the surrounding water phantom when Gd atoms are homogenously distributed in the cell. In the first 0.1 mm (16 times the cell radius for a 6 μm radius cell) the major contribution to the absorbed dose is from IC electrons. Passed this length, the contribution from prompt gamma increases and dominates the absorbed dose. The neighbouring tumour cells will also get cross-fire dose from prompt gammas. The major drawback is that normal tissue several cm from the capture site receives absorbed dose from gamma radiation.
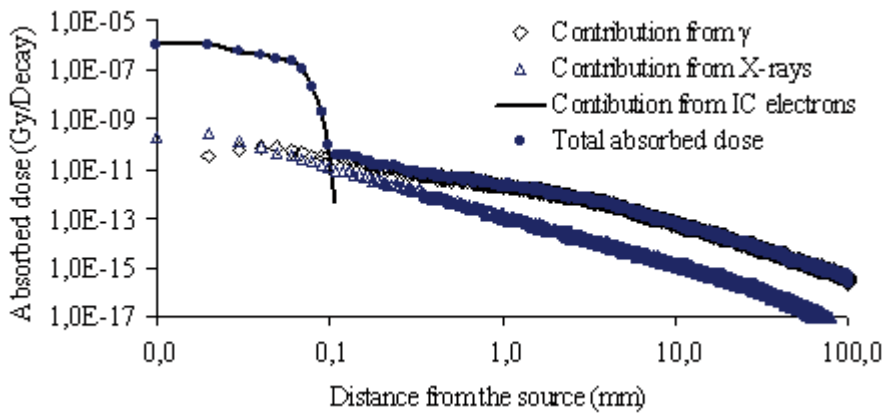

Figure 10. Contribution to the absorbed dose from average energy of different radiation products was calculated in the surrounding water sphere when Gd was homogenously distributed in the cell.

Discussion paper 1-III

The aim of paper I-III was to investigate external neutron activation of Gd for vascular brachytherapy and tumour therapy. The MC method is the method of choice for these kinds of studies. Several MC codes are available and it is not always obvious which code should be used. Since neutron activation studies comprise both hadronic and electro-magnetic interactions several codes with different properties were tested within this project. For neutron transport problem, the commonly used code MCNP has encountered some competition from an object-oriented simulation toolkit, GEANT4, which provides a diverse set of software components that can be employed in different scientific fields.

The first paper is a comparison between calculated results and measurements for thermal neutron capture in Gd using MCNP and GEANT4. Since

the physics is implemented in different ways in the two codes, different results were obtained. One example is that thermal neutron scattering from chemically bound atoms, $S(\alpha,\beta)$ is implemented in MCNP but not in the standard version of GEANT4 for any material. GEANT4 code cannot be trusted for dosimetry calculations in the low-energy neutron medical applications like NCT. MCNP was selected for further Gd neutron capture studies involving the simulation of thermal neutron transport in tissue-like material. However, the open structure of GEANT4 should make it possible to implement thermal neutron scattering for chemically bound atoms.

In the second paper GdNCB is introduced as new treatment method for IVBT which has shown effective to reduce the intimal hyperplasia associated with restenosis following balloon injury. Compared to present techniques, GdNCB offers several advantages. Thermal neutron capture in Gd yields a spectrum of high-energy gamma photons, which due to the build-up effect gives an almost flat absorbed dose delivery pattern around the stent up to 4 mm. To spare normal tissue further, fractionation of the absorbed dose is also possible. The demonstrated higher capture rate at both ends leads to larger absorbed doses which may prevent stent edge and in-stent restenosis. The position of the stent can be verified and corrected by the treatment plan prior to activation. Activation of the stent by an external neutron field can be performed days after catheterisation when the target cells start to proliferate and can be expected to be more radiation sensitive. Another advantage of the non-radioactive Gd stent is the possibility to avoid radiation hazard to personnel.

GdNCR includes both very short (nm) range and long (mm to several cm) range products. In paper III both the microscopic and the macroscopic part of the absorbed dose from GdNCR were investigated for use in GdNCT. In cell studies the emission of prompt gamma will give little contribution to the absorbed dose. In an *in vivo* situation the absorbed dose from prompt gamma will dominates over the dose from IC and Auger electrons. However, Auger electrons can induce double-strand breaks in the DNA if the Gd is attached to or placed within the DNA. The absorbed dose from IC electrons will enhance the total absorbed dose in the tumours and contribute to the cell killing.

New GdNCT compounds using both cell and nucleus internalisation strategies (double-step targeting) could have an effective radiotherapeutic effect on tumour cells. The very small size and optimal Gd packing density of the compounds allows the labelling of matching size targeting molecules and the possibility to more effectively deliver contrast agents to targeted areas in the body. Such targeting techniques could increase the concentration of Gd in tumours and decrease it in the normal tissue preventing the thermal neutron flux depression at the target and also decreasing the absorbed dose to healthy tissue.

30

NCT is in principle an attractive therapy modality but the realisation of the technique involves difficulties, e.g. the delivery of the right quality of neutrons. Present neutron sources deliver mainly epithermal neutrons that are moderated in the tissue to thermal energies, which gives a better tissue penetration depth and dose distribution. The physics around reactor produced neutron fields for NCT has reached a sophistication that is difficult to improve. Some technical progress may still be possible using accelerator produced neutrons but the main advantage here is probably that this technique will allow hospital based therapy with a rotational gantry arrangement.

Targeted radionuclide therapy (Paper IV)

In paper IV estimation of inter-cluster cross-fire radiation dose from β-emitting radionuclides in a breast cancer model was presented in a mathematical model designed on the basis of histological findings. Patients with disseminated breast cancer metastasis that tested positively for over-expression of HER2 receptors are suitable candidates for targeted radionuclide therapy. According to the histological material used in this study primary breast cancers and lymph node metastases were not containing a homogeneous mass of tumour cells. Instead, they contained cell clusters, with a mean size in the range of 18-147 µm, which were spread in a pattern with a distance between closest neighbours ranging in the interval from a few up to more than hundred micrometers as shown in figure 11. This raised the question of how much the spread of cell clusters affects the contribution of cross-fire radiation dose between the clusters.
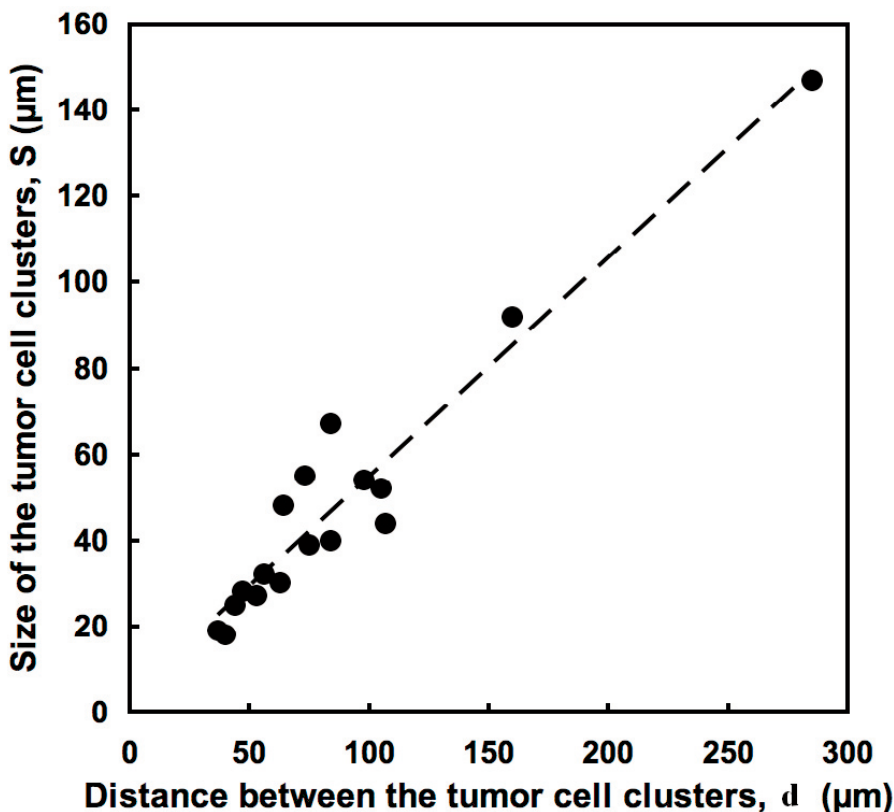
Figure 11. Correlation between average tumour cell clusters sizes, S, and average distances between the tumour cell clusters. [48]

The cell clusters were simulated as spheres with 15, 25, 50 μm radius having a homogeneous radioactivity distribution. The self-dose as well as the dose distribution around the spheres were calculated for seven β-emitting radionuclides, ^{90}Y, ^{188}Re, ^{32}P, ^{186}Re, ^{159}Gd , ^{131}I and ^{177}Lu using the GEANT4 code. Figure 12 shows the absorbed dose distribution from a 25 μm radius source, loaded with different β-emitters. The radionuclide with the lowest beta energy, ^{177}Lu, followed by ^{131}I deposits all of the energy in the vicinity of the source while high energetic radionuclides, such as ^{188}Re and ^{90}Y, deposited their energy up to 1 cm away from the source.

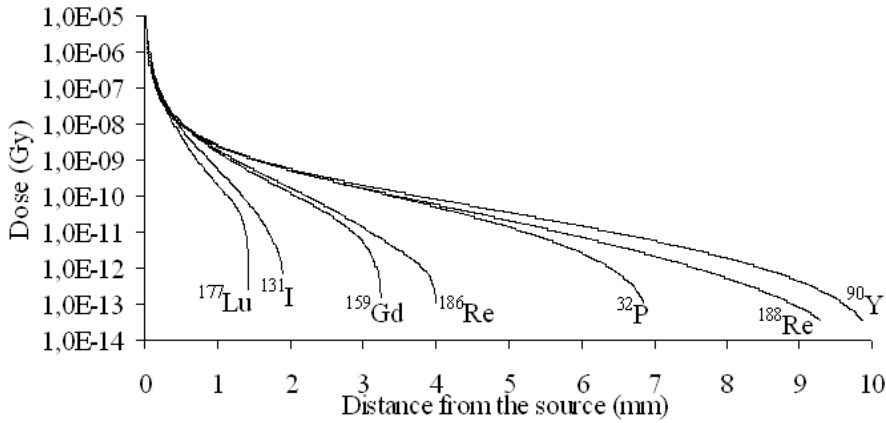Figure 12. The absorbed dose distribution in surrounding water per emitted β particle as a function of distance from a 25 μm radius source loaded with the β-emitters. [48]

The self-absorbed energy in spheres with 15, 25 and 50 μm radii as a fraction of the total released decay energy is shown in table 2. As expected the small volume and the high beta energies gave absorbed fractions well below 1 % while large volumes and low beta energies gave absorbed fractions of well above 10 %.

Table 2. The energy deposited in the cell clusters as a percentage of total deposited energy.

r (μm)	^{90}Y	^{188}Re	^{32}P	^{186}Re	^{159}Gd	^{131}I	^{177}Lu
15	0.25	0.47	0.35	1.36	1.98	3.37	6.01
25	0.42	0.76	0.59	2.18	2.91	5.44	9.56
50	0.84	1.51	1.19	4.25	4.84	10.19	17.70

The inter-cell cluster cross-fire dose from all neighbours was calculated for the β-emitters listed above. The values were divided by the self-dose of the cell cluster and are presented in table 3. The results show clearly that a dominant part of the high beta energy is utilised for cross-fire while for the low beta energy the self-dose is dominant or of equal importance as the cross-fire. An exception was ^{188}Re which, compared to ^{32}P, had higher beta energy as well as higher self-dose.

Table 3. The ratio of inter-cell cluster cross-fire dose from all neighbours and self dose.

r (μm)	^{90}Y	^{188}Re	^{32}P	^{186}Re	^{159}Gd	^{131}I	^{177}Lu
15	208	111	150	38	26	15	8
25	124	69	89	24	17	9	5
50	62	34	43	12	10	5	2

Discussion paper IV

The mathematical model presented in paper IV for estimation of the importance of an inter-cell cluster cross-fire effect was based on histological findings in samples from breast cancer patients and a morphometric analysis. The analysed cell clusters had varying sizes and seemed more or less randomly spread in both in the primary tumours and the lymph node metastases. The main goal of this study was to make an estimate of the magnitude of the cross-fire effect which motivated the use of a simplified model with a limited number of cell cluster sizes (radius of 15, 25 and 50 µm). These values were chosen to represent small, intermediate and large tumour cells. The distance between the cell clusters was selected to be twice the diameter of the cell clusters which was motivated by the results seen in figure 11.

The range of the β-particles is an important factor in the choice of the right β-emitter for targeted radionuclide therapy. If β-range is large, the self-dose will be small but the number of metastases receiving cross-fire dose will increase. As expected, the self-dose increased with decreasing β-energy. Radionuclides with substantial amounts of conversion and Auger electrons tended to deviate from this pattern e.g. ^{188}Re that has higher beta energy than ^{32}P but still a higher self-dose.

Our results shows that, for example, a cell cluster with the radius 15 µm will only absorb a few pro mille of the total released energy in the ^{90}Y-decay while about six percent is absorbed in the decay of ^{177}Lu. There is no doubt that ^{177}Lu is the radionuclide of choice to treat single cells or a micro-metastases homogeneously containing tumour cells. However, in a clustered metastasis or primary tumour, the situation is different and the cross-fire effect of higher β-energy particles might here be beneficial. The results support the idea that an effective therapy approach may be a combination of radionuclides where the high self-dose from nuclides with low β-energy should be combined with the inter-cell cluster cross-fire dose from high-energy β-particles. However, with the long particle range of ^{32}P, ^{188}Re and ^{90}Y, there is a possibility that normal tissues or critical organs adjacent to the targeted metastases may receive unwanted high radiation doses.

Detector response modelling (Paper V)

Silicon diode detectors are widely used in clinical dosimetry. Silicon is the most commonly used diode material sine it is inexpensive, has a relatively low atomic number, and has favourable semiconductor properties. Silicon diode detectors are provided with encapsulation that must be appropriately chosen depending on the type and quality of the clinical beams. MC calculation is an obvious candidate for such investigations. Since the dimen-

sion of the diodes are very small compared to the surrounding phantom, simulation of hundreds of millions of particle histories is required to achieve reliable results with good statistical accuracy, requiring very large amounts of CPU time. Various VRT such as correlated sampling and importance sampling can be used to make calculations more efficient. The aim of this study was to investigate the effects of the encapsulation materials on the detector response in silicon diodes using the MC technique with variance reduction based on correlated sampling and importance sampling.
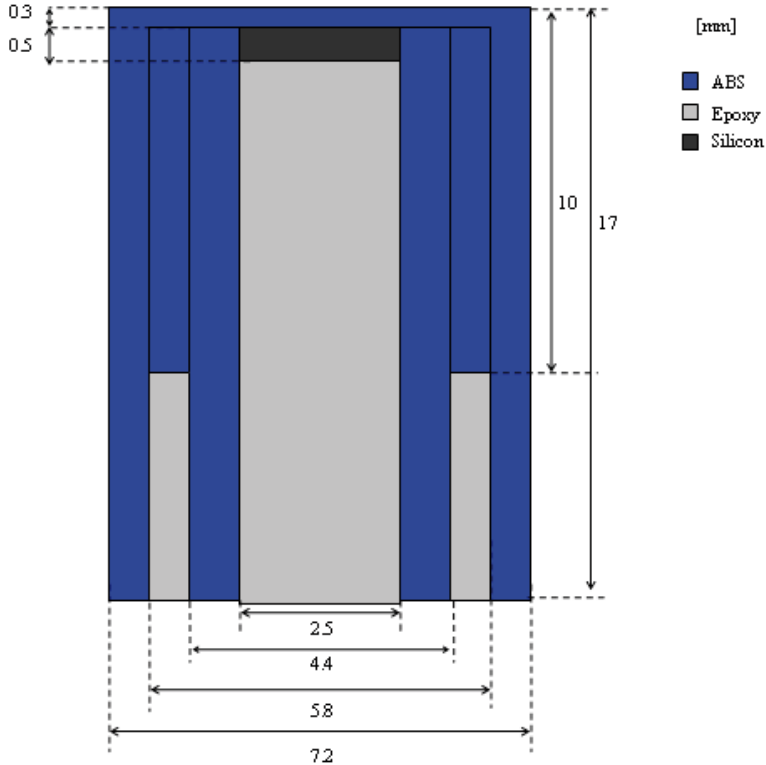
Figure 13. Geometry of the EFD-detector.

Photons of 3 MeV in a circular field of radius 5 cm have been simulated for three geometries: a large water phantom reference case (geometry 1) with a scoring volume consisting of a cylindrical water disc at 10 cm depth of radius 0.125 cm and thickness 0.5 mm, a simple approximation of a silicon diode (geometry 2) by replacing the water in the scoring volume of geometry 1 with silicon, and a realistic representation of a diode detector (geometry 3, figure 13), where the silicon disc as in geometry 2 was encapsulated with epoxy and ABS-plastic (polyAkrylnitrilButadienStryren) to mimic the design of the commercial EFD detector from IBA Dosimetry. Two Monte Carlo packages, Penelope and EGSnrc, were used.
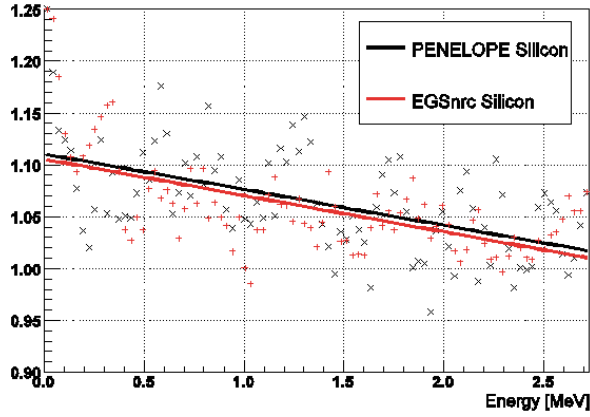
Figure 14. Ratio between electron fluence in scored volume in geometry 1 and 2.

The number of simulated histories was $200 \cdot 10^6$ in all calculations. The benefit from the VRT was an improvement by a factor of four. Figure 14 illustrates the ratio between the electron fluence in the scored water volume in geometry 1 and the silicon disc in geometry 2. The ratio between electron fluence in the scored water volume in geometry 1 and the silicon disc in geometry 3 (EFD) is shown in figure 15.

The ratios in figure 14 are 5% higher than the ratios in figure 15. This indicates that the bare silicon disc influences the spectrum more than the encapsulated disc. The epoxy core behind the silicon disc in the encapsulation seems to attenuate more of the backscattered photons than the case for water. The difference between the simulations is less evident for the high-energy part of the spectrum indicating that the effect on the spectra from the different geometries will be mainly caused by low-energy electrons released by scattered photons. The results show an agreement between the codes within the statistical uncertainties.
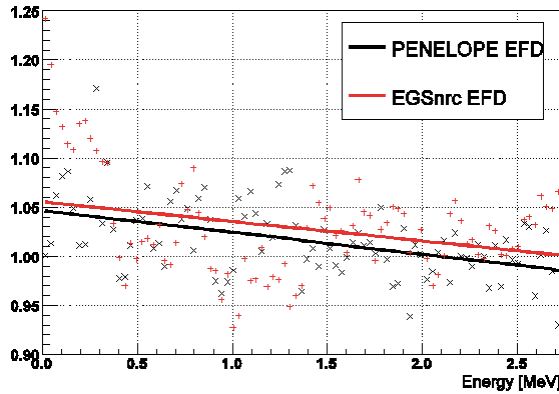

Figure 15. Ratio between electron fluence in scored volume in geometry 1 and 3.

36

Conclusions

With the rapid development in computer technology the use of MC technique has increased and lead to the development of several general purpose codes for radiation transport. In the present thesis EGSnrc, Penelope, MCNP and GEANT4 MC codes have been applied to different areas in radiotherapy. All the codes can simulate photon and electron transport through complicated geometries and media while only MCNP and GEANT4 manage to simulate neutron transport. MCNP was selected for neutron capture studies involving the simulation of thermal neutron transport in tissue-like material since thermal neutron scattering from chemically bound atoms, $S(\alpha,\beta)$ is implemented in MCNP.

Gadolinium neutron capture brachytherapy

GdNCB is introduced as a new treatment method for IVBT and compared to present techniques it offers several advantages. Thermal neutron capture in Gd yields a spectrum of high-energy gamma photons, which due to the build-up effect gives an almost flat absorbed dose delivery pattern around the stent up to 4 mm. Dose distribution from gamma and charge particle radiation at the edges and inside the stent contributes to a non-uniform dose distribution. This will lead to higher doses to the surrounding tissue and may prevent stent edge and in-stent restenosis.

Gadolinium neutron capture therapy

In cell studies the emission of prompt gamma will give little contribution to the absorbed dose. In an *in vivo* situation the absorbed dose from prompt gamma will dominates over the dose from IC electrons. The absorbed dose from IC electrons will enhance the total absorbed dose in the tumours and contribute to the cell killing. Auger electrons can induce double-strand breaks in the DNA if the Gd is attached to or placed within the DNA.

Due to large Gd neutron absorption cross section there is a significant amount of thermal neutron fluence depression even at small amounts of Gd compound present. New GdNCT compounds using both cell and nucleus internalisation strategies (double-step targeting) could have an effective ra-

diotherapeutic effect on tumour cells. The very small size and optimal Gd packing density of the compounds allows the labelling of matching size targeting molecules and the possibility to more effectively deliver contrast agents to targeted areas in the body. Such targeting techniques could increase the concentration of Gd in tumours and decrease it in the normal tissue preventing the thermal neutron flux depression at the target and also decreasing the absorbed dose to healthy tissue.

Targeted radionuclide therapy

The range of the β-particles is an important factor in the choice of the right β-emitter for targeted radionuclide therapy. If β-range is large, the self-dose will be small but the number of metastases receiving cross-fire dose will increase. The self-dose increased with decreasing β-energy except for the radionuclides with substantial amounts of conversion electrons and Auger electrons e.g. ^{188}Re that has higher beta energy than ^{32}P but still a higher self-dose.

An effective therapy approach may be a combination of radionuclides where the high self-dose from nuclides with low β-energy should be combined with the inter-cell cluster cross-fire dose from high-energy β-particles. However, with the long particle range there is a possibility that normal tissues or critical organs adjacent to the targeted metastases may receive unwanted high radiation doses.

Detector response modelling

Monte Carlo simulations using correlated sampling together with importance sampling effectively work to within the small volume of silicon diode detectors calculate spectra perturbations caused by the silicon chip and its encapsulation. Penelope and EGSnrc were used and yielded similar results within the statistical limits. The low-energy part of the electron spectrum was higher in silicon than in water, but less higher for the encapsulated chip than for the bare chip indicating that the epoxy backing of almost 2 cm filter out a significant amount of scattered photons that otherwise would have released low-energy electrons in the chip.

The results from this study suggest that dosimetric calculations using spectra under the assumption that it is unperturbed by a detector would benefit from taking into account the effects on the scattered radiation from the surrounding materials. To understand the effects, further studies of the different components of the electron spectra are necessary and will be attended in a future study.

Summary in Swedish

Strålterapi används för behandling av cancer som monoterapi eller i kombination med kirurgi och kemoterapi. Strålning kan även användas inom andra områden, till exempel för att hindra re-stenos efter ballongvidgning. Avsikten med strålbehandling är att bota eller lindra genom att ge en tillräckligt hög och jämn dos till hela behandlingsvolymen, samtidigt som bestrålning av närliggande frisk vävnad minimeras. Behandling med externa strålkällor är den vanligaste formen av behandling men andra behandlingsformer såsom brachyterapi och målsökande terapiformer med kemiska agens förekommer också. Vid behandling med brachyterapi placeras strålkällan nära eller i tumören, och kallas intrakavitär behandling om strålkällan placeras i en kroppshålighet eller interstitiell behandling om strålkällan förs in i tumörvävnaden. Fördelen med denna metod är att strålkällan följer behandlingsvolymen (målet) vid organrörelser. Vid målsökande strålterapi bestrålas tumörcellerna selektivt genom att koppla radionuklider till lämpliga molekyler som binder specifikt till strukturer som uttrycks på tumörcellerna.

Strålningens växelverkan med materia är komplex och kräver sofistikerade beräkningsmetoder. För att simulera hur partiklar (både laddade och oladdade) växelverkar med materia användes program som baseras på Monte Carlo-metoden (MC), en sannolikhetsbaserad beräkningsmetod, som utgår från grundläggande fysikaliska egenskaper.

Jämförelse mellan olika MC-program och experimentella data är nödvändig, då de flesta av programmen använder sig av olika växelverkansbibliotek och transportmodeller som kan orsaka en viss skillnad i resultaten. I den här avhandlingen används MC-programmen EGSnrc, Penelope, MCNP och GEANT4 i olika områden inom strålterapin. Alla dessa program kan simulera foton- och elektrontransporten genom komplicerade geometrier och materia medan bara MCNP och GEANT4 kan simulera neutrontransport. MCNP valdes för termisk neutrontransport i vävnadsliknande material eftersom termisk neutronspridning från kemisk bundna atomer, $S(\alpha,\beta)$ är implementerad i MCNP men inte i GEANT4.

Gadolinium i brachyterapi och tumörterapi

Bakgrund

Neutroninfångningsterapi är en strålningsterapeutisk metod där patienten ges ett neutroninfångande ämne som kan ackumuleras signifikant i behandlingsområdet och bestrålas sedan med termiska neutroner. Bara ett fåtal nuklider är lämpliga för neutroninfångningsterapi. Borisotopen ^{10}B har använts mest på grund av dess höga tvärsnitt för termiska neutroner (3800 barn). Gd är en annan nuklid som har föreslagits för användning inom neutroninfångningsterapin och används idag frekvent som kontrastmedel vid kliniska MRI-undersökningar. Tvärsnittet för infångning av termiska neutroner hos naturligt Gd (49 000 barns) domineras av ^{157}Gd (254 000 barns), vilket är det största existerande tvärsnittet för infångning av termiska neutroner, och är 60 gånger mer än ^{10}B. Vid infångning av termiska neutroner i ^{157}Gd skickas en kaskad av prompt gammastrålning ut med efter följande utstrålning av konversion- och Auger elektroner. Räckvidden på dessa partiklar sträcker sig från cm till nm.

Brachyterapi

Stenos är en folksjukdom som innebär förträngningar i blodkärl, främst hjärtats kranskärl. Som terapi används i dag rutinmässigt sk ballongteknik för att vidga kärlen. En teknik för att minska risken för att kärlen kollapsar efter ingreppen är att lägga in ett metall nät, ett s.k. stent. I samband med balkongvidgning skadas blodkärlet och under läkningsprocessen finns det en risk att så många nya epitelceller produceras att kärlet ånyo täpps till och vi får en s.k. re-stenos. Brachyterapi kan användas för att bestråla de delande cellerna för att minska deras tillväxthastighet. Vi har föreslagit Gd-neutroninfångningsbrachyterpi som en ny behandlingsmetod. Jämfört med dagens brachyterapi teknik erbjuds följande fördelar:

- Stentets läge relativ stenos och behandlingsområde kan bestämmas med t.ex. datortomografi.
- Det dröjer 2-3 dagar innan läkningsprocessen startar. Cellerna börjar då dela på sig och det är först i detta skede som de börjar bli mer strålkänsliga än omgivningen. Genom att slå på strålningen vid detta tillfälle kan högre önskad biologisk effekt erhållas med mindre dos och därmed risken för strålskador i kärlväggen och risken för sena komplikationer minskar.
- Eftersom stentet ligger permanent på plats kan det när som helst vid kliniska indikationer på begynnande hopväxt av kärlet aktiveras utifrån med neutroner och på detta sätt få en lokal bestrålning av behandlingsområdet.

- Högenergetiska fotoner från Gd ger en mycket bättre dosfördelning kring kärlet. Den absorberade dosen är jämn de första 4 mm runt stentet.

Tumörterapi

I cellstudier kommer bidragen från prompt gamma till absorberad dos att vara väldigt liten jämfört med dosen från konversionselektroner medan i en *in vivo* situation kommer absorberad dos från prompt gamma att dominera över dosen från konversionselektroner. Absorberad dos från konversionselektroner kommer dock att öka den totala dosen i tumören och bidra till celldöd. Auger elektroner kommer att kunna inducera dubbelsträngbrott i DNA om Gd är bunden till DNA. Även små mängder Gd i vävnad kan orsaka termisk neutronflödesminskning på grund av dess stora tvärsnitt för infångning av termiska neutroner. För stora tumörer kan det innebära en ojämn dosfördelning genom tumören. Förekomsten av Gd i normal vävnad kan bidra till termisk flödesminskning och lägre dos till tumören.

Målsökande radionuklidterapi

Bröstcancer är en av de vanligaste cancerformen bland kvinnor. Enligt den statistik som finns har omkring en tredjedel av svenska patienter metastaser som upptäcks samtidigt med cancern. Ytterligare en tredjedel beräknas ha så små metastaser, mikrometastaser, att de inte hittas när cancern upptäcks. Ett sätt att lokalisera och behandla dessa mikrometastaser är att använda målsökande terapiformer med molekyler (målsökare) som binder till strukturer som i idealfallet endast finns på tumörceller och inte på friska celler. Till dessa målsökare kan man sedan koppla en radionuklid som orsakar celldöd.

I studie fyra har utifrån histologisk material en matematisk modell utvecklats för att beräkna korsbestrålningen mellan mikrometastaser från ett antal β-strålande radionuklider med hjälp av MC-programmet GEANT4. Räckvidden på β-partikeln är en viktig faktor för bestämning av rätt β-strålare för målsökande radionuklidterapi. β -partiklar med lång räckvidd kommer att ge väldigt lite självdos (dos till metastasen som β-partikeln är bunden till), medan antal grannmetastaser som får korsbestrålning ökar. Självdosen ökar med minskande β-energi, med undantag för radionuklider med en betydande mängd konversion och Auger elektroner.

En effektiv behandlingsmetod kan vara en blandning av β-strålare med kort räckvidd, som kan ge en hög självdos och lång räckvidd som kan ge korsbestrålning till grannmetastaserna.

Modellering av detektor respons

För en bra strålbehandling är det viktigt att strålningen riktas mot ett bestämt behandlingsområde och doseras rätt. I enlighet med internationella rekommendationer bör behandlingsdosens osäkerhet inte överstiga 5 %. För att kunna uppfylla detta krav krävs det effektiva verktyg och metoder för dosimetri och kvalitetssäkring för att bekräfta att given dos är detsamma som dosen uträknat med dosplaneringssystemet. Den givna dosen verifieras genom mätningar av stråldos i fantom (*in vitro*) och direkt under patient bestrålningen (*in vivo*). Dioddetektorer kan användas både i *in vitro* och *in vivo*-dosimetrin med kisel som det vanligaste diodmaterialet. Kiseldioder som används för dosimetri inom kvalitetssäkring är försedda med inkapslingsmaterial som väljs beroende på stråltyp. MC-metoden erbjuder tekniker för undersökning av inverkan på detektorns respons från dessa inkapslingsmaterial.

I studie fem har MC-programmen EGSnrc och Penelope används för att undersöka spektralpåverkan från inkapslingen på en kommersiell dioddetektor från IBA Dosimetry.

Acknowledgements

References

1. Janicki C, Duggan DM, Gonzales A, Dose model for a beta-emitting stent in a realistic artery consisting of soft tissue and plaque, Med. Phys. 26:2451-2460 (1999).

2. Reynaert N, Verhaegen F, Taeymans Y, Eijkeren MV, Thierens H, Monte Carlo calculations for dose distribution around ^{32}P and ^{198}Au stents for intravascular brachytherapy, Med. Phys. 26:1484-1491 (1999).

3. Amols HI, Zaider M, Weinberger J, Ennis R, Schiff PB, Reinstein LE, Dosimetric considerations for catheter-based beta and gamma emitters in the therapy of neointimal hyperplasia in human arteries, Int. J. Radiat. Oncol. Biol. Phys. 36:913-921 (1996).

4. Patel NS, Chiu-Tsao ST, Ho Y, Duckworth T, Shih JS, Tsao HS, H Quon, Harrison LB, High beta and electron dose from ^{192}Ir: Implications for "gamma" intravascular brachytherapy, Int. J. Radiat. Oncol. Biol. Phys. 54:972-980 (2002).

5. Nath R, Amols H, Coffey C, Duggan D, Jani S, Li Z, Schell M, Soares C, Whiting J, Cole PE, Crocker I, Schwartz R, Intravascular brachytherapy physics: Report of the AAPM Radiation Therapy Committee Task Group No. 60, Med. Phys. 26:119-152 (1999).

6. Carlsson J, Aronsson EF, Hietala SO, Stigbrand T, Tennvall J Tumour therapy with radionuclides: assessment of progress and problems. Radiother. Oncol. 66:107-117 (2003).

7. DeNardo SJ, Tumor-Targeted Radionuclide Therapy: Trial Design Driven by Patient Dosimetry. J. Nucl. Med. 41:104-106 (2005).

8. Larson SM, Krenning EP, A Pragmatic Perspective on Molecular Targeted Radionuclide Therapy. J. Nucl. Med. 46:1-3 (2005).

9.   Kassis AI, Adelstein SJ, Radiobiologic Principles in Radionuclide Therapy. J. Nucl. Med. 46:4-12 (2005).

10.   Kawrakow I and Rogers DWO, The EGSnrc code system: Monte Carlo simulation of electron and photon transport, Technical Report PIRS-701, National Research Council of Canada (2000).

11.   Baro J, Sempau J, Fernandez-Varea JM, and Salvat F, PENELOPE: an algorithm for Monte Carlo simulation of the penetration and energy loss of electrons and positrons in matter, Nucl. Inst. Meth. B100: 31– 46 (1995).

12.   Briesmeister F, MCNP-A General Monte Carlo N-Particle Transport Code, LA-12625-M, Version 4B (1997).

13.   Agostinelli et al., Geant4—a simulation toolkit, Nucl. Inst. Meth. A506: 250–303 (2003).

14.   Lövqvist A, Emanuelsson H, Nilsson J, Lundqvist H, Carlsson J, Pathophysiological mechanisms for restenosis following coronary angioplasty: possible preventive alternatives, J. Intern. Med. 233:215-226 (1993).

15.   Amols HI, Review of endovascular brachytherapy, Physics for prevention of restenosis, Cardiovasc. Radiat. Med. 1:64-71 (1999).

16.   Bailey SR, Drug-eluting stents have made Brachytherapy obsolete, Curr. Opin. Cardiol. 19: 598-600 (2004).

17.   Yuan J, Jette D, Chen W, Deterministic photon kerma distribution based on the Boltzmann equation for external beam radiation thrapy, Med. Phys. 35: 4079-4086 (2008).

18.   Vassiliev ON et al, Feasibility of a multigroup deterministic solution method for three-dimensional radiotherapy dose calculations, Int. J. Radiation Oncology Biol. Phys. 72: 220-227 (2008).

19.   Bielajew AF, Fundamentals of the Monte Carlo method for neutral and charged particle transport (2001).

20.   P. Andreo, Monte Carlo technique in medical radiation physics, Phys. Med. Biol. 36:861-920 (1991).

21.   Rogers DWO, Monte Carlo Techniques in Radiotherapy, Physics in Canada, Medical Physics Special Issue, 58:63–70 (2002).

22.   Ahnesjö A, Aspradakis MM, Dose calculations for external photon beams in radiotherapy, Phys. Med, Biol. 44:99-155 (1999).

23.   Rodgers JE, Monte Carlo simulations of dose deposition applied to clinical radiation Therapy, Rad. Meas. 41:36–44 (2007).

24.   Raeside DE, Monte Carlo principles and applications, Phys. Med. Biol. 21: 181–197 (1976).

25.   Sheikh-Bagheri D, Kawrakow I, Walters B, Rogers DWO, Monte Carlo Simulations: Efficiency Improvement Techniques and Statistical Considerations, Integrating New Technologies into the Clinic: Monte Carlo and Image-Guided Radiation Therapy - Proc. of AAPM Summer School: 71-91 (2006).

26.   Bielajew AF and Rogers DWO, Variance-reduction techniques, in Monte Carlo Transport of Electrons and Photons, edited by Jenkins T, Nelson W, Rindi A, Nahum A, and Rogers D, Plenum, New York, 407–419 (1989).

27.   Kawrakow I, Rogers DWO and Walters B, Large efficiency improvements in BEAMnrc using directional bremsstrahlung splitting, Med. Phys. 31:2883–2898 (2004).

28.   Kawrakow I and Fippel M, Investigation of variance reduction techniques for Monte Carlo photon dose calc lation using XVMC , Phys. Med. Biol. 45:2163–2184 (2000).

29.   Buckley LA, Kawrakow I, and Rogers DWO, "CSnrc: Correlated sampling Monte Carlo calculations using EGSnrc," Med. Phys. 31:3425-3435 (2004).

30.   Sempau J, Andreo P, Aldana J, Mazurier J, Salvat F, Electron beam quality correction factors for plane-parallel ionization chambers: Monte Carlo calculations using the PENELOPE system, Phys. Med. Biol. 49:4427–4444 (2004).

31.   Ma CM, Nahum AE, Calculation of absorbed dose ratios using correlated Monte Carlo sampling, Med. Phys. 20:1189–1199 (1993).

32.   Bielajew AF, Correction factors for thick-walled ionization chambers in point source photon beams, Phys. Med. Biol. 35:501–516 (1990).

33.   Berger M. J. et al, Photon Cross Sections Database XCOM (1998).

34.   Cullen D. E, Hubbell J.H. and Kissel L., EPDL97: The evaluated photon data library, 97 version. *Lawrence Livermore National Laboratory Report UCRL-50400* 6 (1997).

35.   Ribberfors R., Relationship of the relativistic Compton cross section to the momentum distribution of bound electron states. *Physical Review B,* 12**,** 2067 (1975a).

36.   Ribberfors R., Relationship of the relativistic Compton cross section to the momentum distribution of bound electron states. II. Effects of anisotropy and polarization. *Physical Review B,* 12**,** 3136 (1975b).

37.   Ribberfors R. X-ray incoherent scattering total cross sections and energy-absorption cross sections by means of simple calculation routines. *Physical Review A,* 27**,** 3061 (1983).

38.   Storm E., and Israel H. I., Photon Cross Sections from 1 keV to 100 MeV for Elements Z=1 to Z=100. *Atomic Data and Nuclear Data Tables,* 7**:** 565-681 (1970).

39.   Attix FH, *Introduction to radiological physics and radiation dosimetry*, Wiley, New York, (1986).

40.   Berger MJ, Monte Carlo calculation of the penetration and diffusion of fast charged particles, in *Methods in Comput. Phys.*, edited by Alder B , Fernbach S, and Rotenberg M, Academic, New York, 1:135–215 (1963).

41.   Fernández-Varea J. M., Mayol R., Baro J., and Salvat F., On the theory and simulation of multiple elastic scattering of electrons, Nucl. Instrum.Methods Phys. Res. B, 73: 447–473, (1993).

42.   Verhaegen F and Seuntjens J, Monte Carlo modelling of external radiotherapy photon beams, Phys. Med. Biol. 48**:**107-164 (2003).

43.   D. E. Cullen *et al.*, "How accurately can we calculate thermal systems?," University of California, UCRL-TR-203892, Lawrence Livermore National Laboratory.

44.   G. L. Locher, "Biological effects and therapeutic possibilities of neutrons," Am. J. Roentgenol. Radium Ther. 36: 1–13 (1936).

45.   J. Stepanek, "Emission spectra of gadolinium-158," Med. Phys. 30: 41–43 (2003).

46.   S.A. Enger, P. Munck af Rosenschöld, A. Rezaei, H. Lundqvist," Monte Carlo calculations of thermal neutron capture in gadolinium: a comparison of GEANT4 and MCNP with measurements," Med Phys. 33:337-41 (2006).

47   S.A. Enger, A Rezaei, Munck af Rosenschöld , H. Lundqvist, "Gadolinium neutron capture brachytherapy (GdNCB), a new treatment method for intravascular Brachytherapy," Med Phys. 33:46- 51 2006.

48   S.A. Enger, T. Hartman, J. Carlsson, H.Lundqvist, "Cross-fire doses from ß-emitting radionuclides in targeted radiotherapy. A theoretical study based on experimentally measured tumor characteristics," Phys. Med. Biol. 53:1909-1920 (2008).

Acta Universitatis Upsaliensis

Digital Comprehensive Summaries of Uppsala Dissertations
from the Faculty of Medicine 375

Editor: The Dean of the Faculty of Medicine

A doctoral dissertation from the Faculty of Medicine, Uppsala University, is usually a summary of a number of papers. A few copies of the complete dissertation are kept at major Swedish research libraries, while the summary alone is distributed internationally through the series Digital Comprehensive Summaries of Uppsala Dissertations from the Faculty of Medicine. (Prior to January, 2005, the series was published under the title "Comprehensive Summaries of Uppsala Dissertations from the Faculty of Medicine".)